Cyst Ventilation Heterogeneity and Alveolar Airspace Dilation as Early Disease Markers in Lymphangioleiomyomatosis

Laura L. Walkup[1,2]*, David J. Roach[1]*, Chase S. Hall[3], Nishant Gupta[4], Robert P. Thomen[1‡], Zackary I. Cleveland[1,2], Francis X. McCormack[4], and Jason C. Woods[1,2]

[1]Center for Pulmonary Imaging Research, Division of Pulmonary Medicine and Department of Radiology, Cincinnati Children's Hospital Medical Center, Cincinnati, Ohio; [2]Department of Pediatrics, [3]Department of Radiology, and [5]Division of Pulmonary, Critical Care, and Sleep Medicine, Department of Internal Medicine, University of Cincinnati College of Medicine, Cincinnati, Ohio; and [4]Division of Pulmonary and Critical Care, University of Kansas Health System, Kansas City, Kansas

ORCID IDs: 0000-0002-5060-6401 (L.L.W.); 0000-0001-9112-1315 (N.G.).

Abstract

Rationale: Lymphangioleiomyomatosis (LAM) is a rare disease associated with cystic destruction of the pulmonary parenchyma and chronic respiratory failure, and there are trials underway to determine if early intervention can prevent disease progression. An imaging technique that is sensitive to early regional disease would therefore be valuable for patient care and clinical trials.

Objectives: We postulated that hyperpolarized ^{129}Xe MRI would be sensitive to ventilation abnormalities and alveolar airspace dilation in patients with mild LAM disease and normal pulmonary function and that ^{129}Xe MRI would reveal important features of cyst ventilation.

Methods: ^{129}Xe ventilation and diffusion-weighted MR images were acquired in 22 patients with LAM during two breath-holds of hyperpolarized ^{129}Xe. ^{129}Xe ventilation defect percentage (VDP; percentage of voxels <60% of the mean whole-lung ^{129}Xe MRI signal) and apparent diffusion coefficient (ADC), a measure of alveolar airspace size, were quantified and compared with pulmonary function test parameters with Spearman statistics. Sixteen patients with LAM had a recent, clinical chest computed tomography (CT) scan available, and cyst ventilation was assessed by thresholding cysts on the CT images and registration to the ^{129}Xe ventilation images.

Results: Ventilation deficits were observed in all patients with LAM, including those with normal pulmonary function and few cysts, and the mean VDP was 19.2% (95% confidence interval [CI], 14.8–23.5%). ^{129}Xe VDP was strongly correlated with forced expiratory volume in 1 second (FEV_1)/forced vital capacity (FVC) ratio ($r = -0.51$, $P = 0.02$) and diffusing capacity of the lung for carbon monoxide (D_{LCO}) ($r = -0.60$, $P = 0.009$) but not with FEV_1 ($r = -0.33$, $P = 0.13$), likely because of the sensitivity of ^{129}Xe MRI to mild LAM disease in patients with normal FEV_1. The mean ADC was 0.048 cm^2/s (95% CI, 0.042–0.053 cm^2/s). In many cases, ADC was elevated relative to previously reported values in adults, and ADC was correlated with FEV_1, FEV_1/FVC ratio, and D_{LCO} ($P \leq 0.02$ for all). Co-registered ^{129}Xe MRI and CT imaging revealed considerable ventilation heterogeneity within individual patients with LAM and across patients with similarly sized cysts.

Conclusions: ^{129}Xe MRI provides a means to assess the complex regional ventilation and alveolar airspace size changes of LAM with high sensitivity and may be a clinically useful future tool for screening, managing patients, and measuring treatment efficacy.

Keywords: hyperpolarized xenon; magnetic resonance imaging; cyst; ventilation

(Received in original form December 11, 2018; accepted in final form April 8, 2019)

*Co–first authors.

‡Present address: Department of Radiology, University of Missouri, Columbia, Missouri.

Supported by the LAM Foundation, University of Cincinnati Center for Clinical & Translational Science & Training, and the Cincinnati Children's Hospital Medical Center Research Foundation.

Author Contributions: Study concept and design: L.L.W., D.J.R., Z.I.C., N.G., F.X.M., and J.C.W.; acquisition, analysis, or interpretation of data: all authors; drafting of the manuscript: L.L.W., D.J.R., R.P.T., and J.C.W.; critical revision of the manuscript for important intellectual content: all authors; statistical analysis: L.L.W., D.J.R., C.S.H., and J.C.W.; study supervision: all authors.

Correspondence and requests for reprints should be addressed to Laura L. Walkup, Ph.D., Cincinnati Children's Hospital Medical Center, Division of Pulmonary Medicine, 3333 Burnet Avenue, MLC 5033, Cincinnati, OH 45229. E-mail: Laura.Walkup@cchmc.org.

Ann Am Thorac Soc Vol 16, No 8, pp 1008–1016, Aug 2019

DOI: 10.1513/AnnalsATS.201812-880OC
Internet address: www.atsjournals.org

Lymphangioleiomyomatosis (LAM), a rare lung disease primarily affecting women of childbearing age, is characterized by abnormal smooth muscle–like cell infiltration leading to cystic parenchymal remodeling and progressive decline in pulmonary function. The currently proposed mechanisms of cyst formation range from ball-valve obstruction and overinflation of small airways to remodeling due to LAM cell–mediated matrix metalloproteinase release or lymphangiogenic remodeling. LAM manifests clinically as increased airflow obstruction and diminished pulmonary function, which is primarily assessed using the parameters of forced expiratory capacity in one second (FEV_1) and diffusing capacity of the lung for carbon monoxide (D_{LCO}). The presence of characteristic diffuse thin-walled cysts on high-resolution chest X-ray computed tomography (CT) imaging plays a central role in establishing the diagnosis of LAM (1–3).

CT imaging methods have been developed to quantify the degree of cystic change in LAM in much the same way as the widely accepted −950 Hounsfield unit (HU) threshold has been used to quantify emphysema on inspiratory CT (4), and, indeed, thresholds of −950 HU (5) and −900 HU (6) have been shown to correlate with clinical measures of LAM severity as assessed by pulmonary function tests (PFTs). Additional studies have supported the use of quantitative CT imaging techniques as novel biomarkers for monitoring LAM progression, as well as assessing treatment response and mechanism of therapeutic action (7–9); however, the enthusiasm for CT imaging as a longitudinal disease-monitoring tool is dampened because of the risks associated with cumulative ionizing radiation exposure. Furthermore, CT scans do not provide functional or regional information about the ventilation of LAM cysts, which impacts dead-space ventilation and likely relates to the risk of pneumothorax. Ventilation/perfusion (V/Q) scanning has some limited utility in that regard, and in a study of patients with LAM, a "speckling pattern" in the ventilation images was attributed to accumulation of radiotracer within the LAM cysts (10). However, V/Q scintigraphy is associated with the risks of ionizing radiation, is only semiquantitative, offers limited sensitivity and tomographic resolution, and cannot provide useful information about ventilation of individual LAM cysts.

In recent years, many of the technological challenges that have limited magnetic resonance imaging (MRI) of the lungs have been overcome, and MRI has emerged as a "new," nonionizing modality for pulmonary imaging. In addition to remarkable advances in conventional ^{1}H MRI using ultra-short echo-time techniques (11–16), hyperpolarized ^{129}Xe MRI has been shown to be a powerful tool not only for identification of the earliest manifestations of airflow obstruction and ventilation deficits but also for the assessment of alveolar airspace size (17) and gas-exchange dynamics (18). In this technique, the MR signal comes not from the lung parenchyma but from magnetized ^{129}Xe gas, which is inhaled and imaged during a brief breath-hold (18, 19). Over the past 30 years, hyperpolarized ^{129}Xe MRI has been used to spatially resolve and quantify lung ventilation in multiple airway disorders, including cystic fibrosis (20–23), asthma (23, 24), and chronic obstructive pulmonary disease (COPD) (23, 25, 26), and has been shown to be more sensitive to early lung disease than spirometry.

We hypothesized that ^{129}Xe MRI would be sensitive to early cystic lung changes in patients with LAM with normal spirometry and that co-registered ^{129}Xe MRI and CT imaging would reveal important structure–function features of cysts in LAM. Advantages of this novel hyperpolarized-gas technique include spatial resolution of ventilation that is not possible with PFTs, absence of ionizing radiation exposure, sensitivity to the earliest manifestations of airflow obstruction, status as the only available method to measure airspace dimensions *in vivo*, and potential as an effort-independent biomarker of disease progression and treatment response. Portions of this work have been previously presented as abstracts (27, 28).

Methods

Inclusion Criteria

U.S. Food and Drug Administration investigational new drug (IND 123577) and local institutional review board approvals were obtained for all ^{129}Xe MRI studies. Twenty-two patients with LAM (Table 1) were recruited from the University of Cincinnati Pulmonary Clinics and the 2016 Rare Lung Disease Consortium meeting in Cincinnati, Ohio, and signed informed consent. Inclusion criteria included a definite diagnosis of LAM on the basis of American Thoracic Society/Japanese Respiratory Society Criteria (3). Patients with a resting baseline pulse oximetry <95%, positive pregnancy test, or standard MRI exclusions (e.g., MR-incompatible metal implants) were excluded. All MR imaging was performed on a Philips 3T Achieva MRI scanner (Philips Healthcare) during a single study visit of approximately 60 minutes.

PFTs including spirometry and D_{LCO} from within 1 year of the MRI visit were collected from patient medical records. If recent spirometry was unavailable, subjects were asked to complete spirometry on the same day as the MRI scanning was done. For the co-registered ^{129}Xe MRI and CT imaging investigation of cyst size and ventilation, archival CT images that had been obtained in the course of standard clinical care were used, if they had been acquired within 1 year of the MRI.

Hyperpolarized ^{129}Xe MRI

A home-built, single-channel, saddle coil tuned to 35.3 MHz was used to acquire all ^{129}Xe MR images (29). Hyperpolarized ^{129}Xe MRI gas (86% ^{129}Xe-enriched; Linde) was prepared using a commercial polarizer (Polarean 9810) and polarized to approximately 20%. Subjects were instructed to exhale to functional residual capacity before inhaling the hyperpolarized ^{129}Xe gas mixture from a Tedlar bag (Jensen Inert Products) equipped with 3/8-inch tubing (Tygon; Saint-Gobain) and mouthpiece (Epsilon Medical Devices). ^{129}Xe ventilation and diffusion-weighted images were acquired during two separate breath-holds of up to 1 L of ^{129}Xe gas. Gas was delivered in the presence of a medical professional, who monitored heart rate and oxygenation throughout the protocol.

^{129}Xe ventilation images were acquired for all 22 patients using a gradient echo scan during a single breath-hold of 500 ml of hyperpolarized ^{129}Xe diluted to 1 L with N_2 gas. MRI parameters included repetition time, 8 milliseconds; echo time, 4 milliseconds; flip angle, 10° to 12°; 10 to 15 slices; voxel size $\approx 3 \times 3 \times 15$ mm^3; scan duration $\leq$ 16 seconds. To measure alveolar airspace size, ^{129}Xe diffusion-weighted images were acquired in 19 patients with LAM during a second breath-hold of 1 L of hyperpolarized ^{129}Xe gas using a 5 b-value

Table 1. Patient demographics, pulmonary function tests, and cystic lung volume from computed tomography imaging

Subject ID	TSC-LAM or S-LAM	Age at MRI (*yr*)	FEV_1% Predicted	FEV_1/FVC (%)	D_{LCO}% Predicted*	Cystic Lung Percentage From CT Scan*
01	S-LAM	25	129	93	109	N/A
02	S-LAM	71	110	78	44	19.8
03	TSC-LAM	29	110	79	86	0.6
04	S-LAM	47	103	72	N/A	1.8
05	S-LAM	49	99	60	N/A	11.7
06	N/A	56	96	75	72	4.3
07	S-LAM	43	96	75	76	2.3
08	S-LAM	38	92	81	82	1.0
09	TSC-LAM	20	92	92	84	N/A
10	S-LAM	53	91	63	67	26.4
11	S-LAM	53	82	66	N/A	3.2
12	S-LAM	47	80	82	76	11.7
13	S-LAM	43	79	90	77	N/A
14	S-LAM	53	71	72	67	N/A
15	S-LAM	62	71	73	N/A	N/A
16	S-LAM	55	60	79	55	15.5
17	S-LAM	45	58	73	74	20.5
18	S-LAM	71	53	55	28	29.7
19	S-LAM	53	53	31	54	25.3
20	TSC-LAM	57	35	36	49	31.0
21	TSC-LAM	64	35	28	23	60.2
22	S-LAM	46	33	31	33	N/A
Mean (95% CI)		49 (44–55)	79 (68–90)	68 (59–76)	64 (54–75)	15.9 (8.0–23.9)

Definition of abbreviations: CI = confidence interval; CT = computed tomography; D_{LCO} = diffusing capacity of the lung for carbon monoxide; FEV_1 = forced expiratory volume in 1 second; FVC = forced vital capacity; LAM = lymphangioleiomyomatosis; MRI = magnetic resonance imaging; N/A = not available; S-LAM = sporadic LAM; TSC-LAM = tuberous sclerosis complex with associated LAM.
*If available from clinical record.

(0, 6.25, 12.5, 18.75, and 25 s/cm^2), bipolar diffusion-sensitizing gradient echo sequence (repetition time, 6.1 milliseconds; echo time, 2.9 milliseconds; flip angle, 5°–10°; diffusion time [Δ], 3.5 milliseconds; lobe duration [Δ], 3.1 milliseconds; 4–8 slices; voxel size $\approx$ 3–7 × 3–7 × 15–30 mm^3; scan duration $\leq$ 16 s).

Image Analysis and Statistics

^{129}Xe images were processed using custom software in MATLAB (Mathworks) and R processing language. ^{129}Xe ventilation images were manually segmented based on ^{1}H images, and deficits in ventilation were identified using a threshold of <60% of the mean whole-lung ^{129}Xe signal and expressed as a ventilation defect percentage (VDP) as previously reported (20). VDPs are expressed as mean ± SD. Using the ^{129}Xe diffusion-weighted images, maps of the ^{129}Xe apparent diffusion coefficient (ADC), a histologically validated surrogate for alveolar airspace size, were generated via a voxel-by-voxel decaying exponential fit of the 5 b-value data.

The regional ^{129}Xe ventilation of LAM cysts was investigated using open-source ITK-Snap (http://www.itksnap.org/ [30]) and Advanced Normalization Tools (ANTs; http://stnava.github.io/ANTs/) software packages. Binary masks of ^{129}Xe ventilation images were registered to binary CT masks of the corresponding subject via ANTs image registration algorithm (antsRegistrationSyN [31]). After the generation of the registered mask, an image transform was applied to warp the ventilation intensity image to the registered mask to obtain the registered ventilation image. A watershed algorithm was applied to the cyst labels, which were obtained from CT images (<−850 HU to −950 HU), via MATLAB to differentiate individual cysts from large areas of cystic lung, where multiple cysts in close proximity coalesce. The watershed cyst labels were then applied to the registered ventilation image. Because of partial-volume effects, cysts <4 voxels in size were eliminated, and the ^{129}Xe signal intensity of cysts within the 4 to 20 voxel size range were scaled according to:

$$XeIntensity_{Scaled} = XeIntensity_{Original} \cdot \frac{1-(1.3t-C_v)}{1.3t}$$

where t is defined as the slice thickness of the hyperpolarized ^{129}Xe ventilation image (i.e., 15 mm) and C_v is defined as the individual cyst volume derived from CT imaging. Finally, cysts were classified into three categories: poor ventilation (<60% of the mean ^{129}Xe signal intensity), average ventilation (≥60%), or hyperventilated (≥200%). The ventilated cyst volumes were expressed as the percentage of the total lung volume. In addition, individual cyst size was quantified, binned into four different sizes (0 to <0.5 ml, 0.5 to <5 ml, 5 to <50 ml, and ≥50 ml) and presented as a percentage of total lung volume.

Means and 95% confidence intervals (CIs) are reported for group variables. Linear regression and Spearman correlation coefficients (r) were used to describe the relationships between variables; $r \geq 0.5$ was considered strong correlation. Two-sided t tests were used to compare ^{129}Xe VDP and ADC differences between patients with early disease (i.e., FEV_1 or $D_{LCO} \geq 80\%$ predicted) and those with moderate to advanced disease (<80% predicted FEV_1 or D_{LCO}). A P value ≤ 0.05 was considered significant for all comparisons.

Results

Subjects and ^{129}Xe MRI Results

Table 1 describes the patient demographics of the 22 patients with LAM studied, whose average age was 49 years (95% CI, 44–55 yr) and mean FEV_1 was 78% (95% CI, 68–90%; range, 33–129%). All subjects tolerated the MRI procedure well, and no related adverse events were reported. Figure 1 highlights ^{129}Xe ventilation heterogeneity and ADC maps in three representative LAM cases across a spectrum of disease severity. ^{129}Xe ventilation patterns were heterogeneous and varied widely among subjects. Ventilation deficits were observed in all 22 patients with LAM, with a mean ^{129}Xe VDP of 19.2% (95% CI, 14.8–23.5%), as compared with ~5% to 7% VDP in a healthy young subject, although slight increases are associated with normal aging (32). ^{129}Xe ADC, which measures the movement of ^{129}Xe atoms

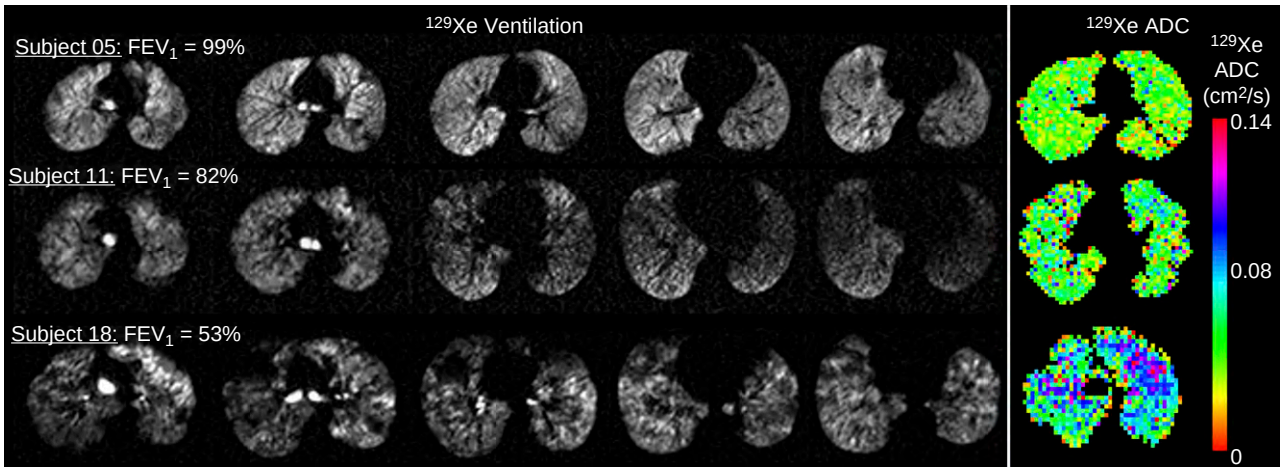

Figure 1. ^{129}Xe ventilation and apparent diffusion coefficient (ADC) maps in three representative lymphangioleiomyomatosis cases demonstrating the spectrum of disease severity investigated. The ^{129}Xe ventilation defect percentage values for subjects 05 (top row), 11 (middle row), and 18 (bottom row) were 14.8%, 15%, and 24.3%, respectively. A single slice of the ADC maps for each of these subjects is shown in the right column. ^{129}Xe ADC, calculated from diffusion-weighted imaging, is a surrogate measurement of alveolar airspace size, and the color bar shows increasing ADC value and thus airspace size. The ^{129}Xe ADC values were 0.040 ± 0.016, 0.048 ± 0.022, and 0.066 ± 0.027 cm^2/s, compared with approximately 0.036 cm^2/s for age-matched healthy adults (17). FEV$_1$ = forced expiratory volume in 1 second.

within the airspace and thus can serve as a surrogate measurement of alveolar airspace size, also varied highly across subjects ($n = 19$), with a mean whole-lung value of 0.048 cm^2/s (95% CI, 0.042–0.053 cm^2/s). Most subjects, including those with normal PFTs, had ^{129}Xe ADC values that were elevated relative to what has been previously reported in healthy adults (~0.036 cm^2/s [17]), suggesting alveolar airspace enlargement even in mild LAM. In more advanced LAM cases, the observed ^{129}Xe ADC was similar to values reported for patients with COPD (0.079 cm^2/s [33]), consistent with advanced cystic lung destruction and airspace dilation. ^{129}Xe VDP was strongly correlated with ^{129}Xe ADC (Figure 2A; $r = 0.60$, $P = 0.007$), supporting the notion that alveolar airspace dilation impedes regional ventilation. ^{129}Xe VDP correlated with the percentage of hyperventilated lung (Figure 2B; $r = 0.86$, $P < 0.001$), suggesting there may be focal regions of hyperventilation to compensate for airflow obstruction.

Correlations with PFTs

The relationships between ^{129}Xe VDP and PFT measurements are shown in Figure 3. ^{129}Xe VDP was strongly correlated with FEV$_1$/FVC ratio ($r = -0.51$, $P = 0.02$) and D_{LCO} ($r = -0.60$, $P = 0.009$), but not with FEV$_1$ ($r = -0.33$, $P = 0.13$). There was wide individual variation in ^{129}Xe VDP across patients with similar PFT-defined disease severity, and, importantly, ventilation deficits were detected in patients with LAM with normal FEV$_1$ (Figure 3A). ^{129}Xe ADC was strongly correlated with FEV$_1$ ($r = -0.51$, $P = 0.02$), FEV$_1$/FVC ratio, ($r = -0.61$, $P = 0.005$), and D_{LCO} ($r = -0.74$, $P < 0.001$).

Sensitivity of ^{129}Xe MRI to Early LAM Disease

Twelve of the 22 patients had mild LAM, with FEV$_1$ ⩾ 80% predicted (Table 1; Subjects 01 through 12), and the group

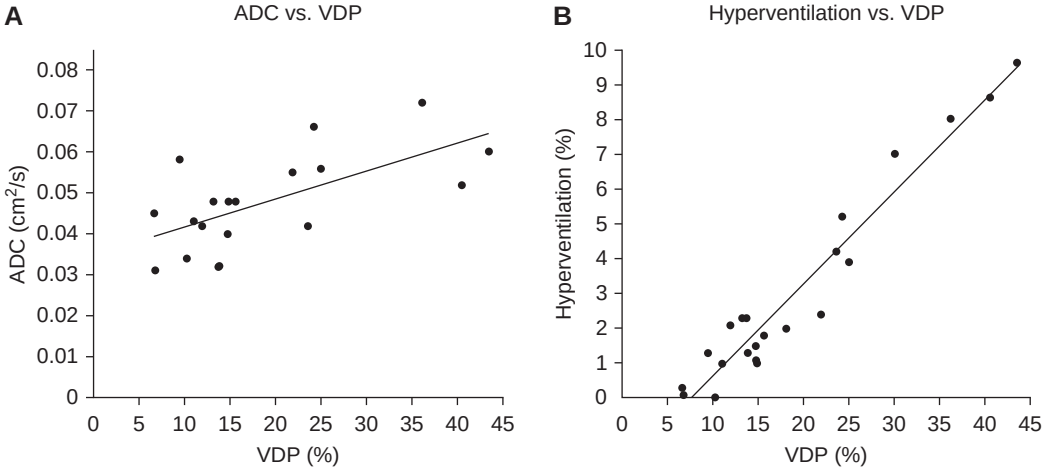

Figure 2. ^{129}Xe ventilation defect percentage (VDP) plotted against ^{129}Xe apparent diffusion coefficient (ADC) (*A*; $r = 0.60$, $P = 0.007$) and the percentage of hyperventilated lung (*B*; $r = 0.86$, $P < 0.001$).

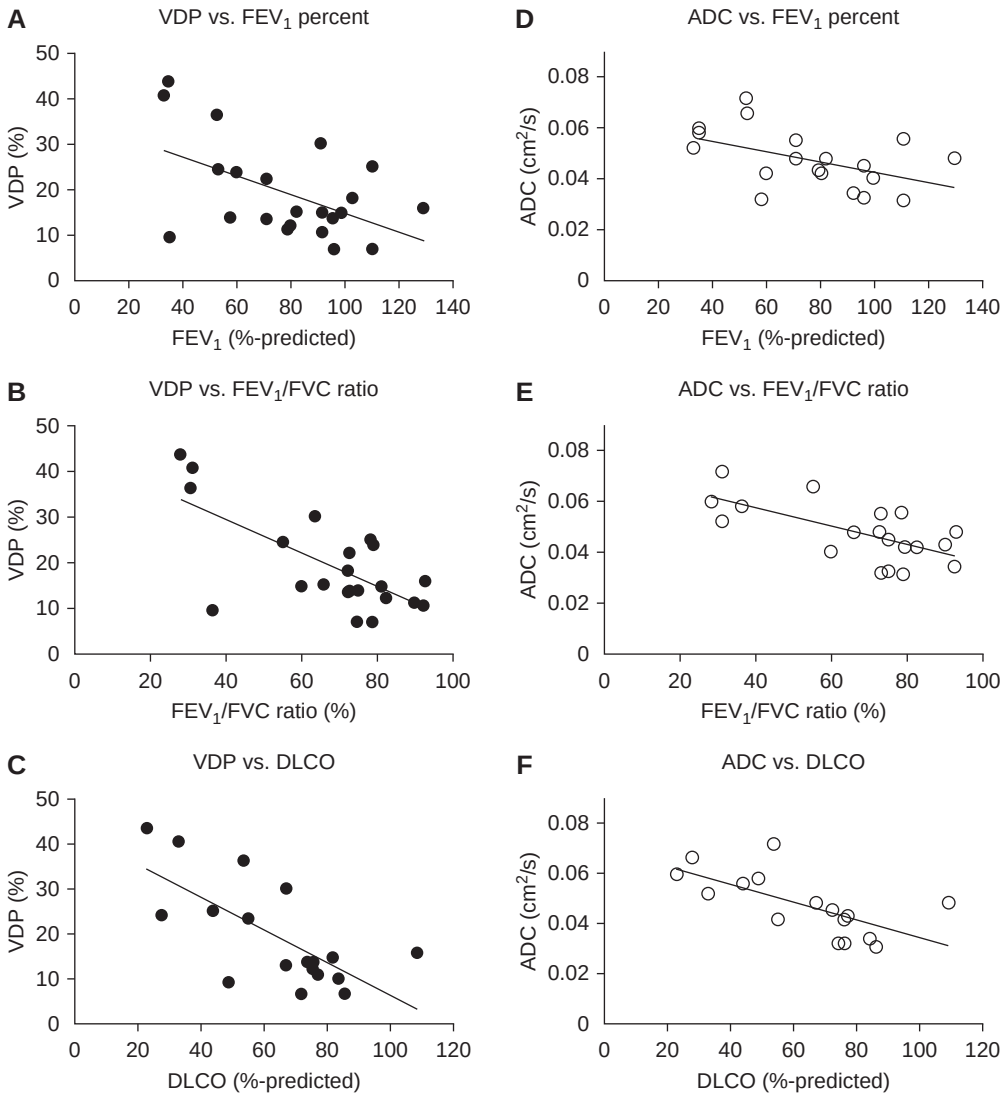

Figure 3. Comparison of ^{129}Xe ventilation defect percentage (VDP; *A*, *B*, and *C*) and apparent diffusion coefficient (ADC; *D*, *E*, and *F*) with forced expiratory volume in 1 second (FEV_1) % predicted (*A* and *D*), FEV_1/forced vital capacity (FVC) ratio (*B* and *E*), and diffusing capacity of the lung for carbon monoxide (D_{LCO}) % predicted (*C* and *F*). D_{LCO} comparisons included the 18 patients with available data. ^{129}Xe VDP was not correlated with FEV_1 ($r = -0.33$, $P = 0.13$) but was correlated with FEV_1/FVC ratio ($r = -0.51$, $P = 0.02$) and D_{LCO} ($r = -0.60$, $P = 0.009$). ^{129}Xe ADC was correlated with FEV_1 ($r = -0.51$, $P = 0.02$), FEV_1/FVC ratio ($r = -0.61$, $P = 0.005$), and D_{LCO} ($r = -0.74$, $P < 0.001$).

mean FEV_1 was 98% (95% CI, 91–106%). Ten patients had moderate to advanced disease, with $FEV_1 < 80\%$ predicted (group mean, 55%; 95% CI, 45–65%). Although there was no statistical difference in the ^{129}Xe VDP of patients with mild disease (mean VDP, 15.3%; 95% CI, 11.4–19.1%) and those with moderate to advanced disease (mean VDP, 23.8%; 95% CI, 16.1–31.5%; $P = 0.07$), this is likely due to the superior sensitivity of ^{129}Xe MRI to early airway obstruction, as supported by the several patients with normal FEV_1 (>80% predicted) yet large ^{129}Xe VDP (Figure 3A). Patients with moderate to advance disease had an elevated ^{129}Xe ADC (mean ADC, 0.053 cm^2/s; 95% CI, 0.045–0.060 cm^2/s) compared with patients with mild disease (mean ADC, 0.042 cm^2/s; 95% CI, 0.036–0.047 cm^2/s; $P = 0.03$), consistent with a greater degree of airspace dilation in subjects with moderate to advanced disease.

When considering disease severity with respect to D_{LCO}, 18 of the 22 patients had available D_{LCO}, and of those 18, 4 patients (Table 1; subjects 01, 03, 08, and 09) had mild disease per the $D_{LCO} \geq 80\%$ predicted definition (group mean, 90%; 95% CI, 78–103%). The mean D_{LCO} for patients with moderate to advanced disease was 57% (95% CI, 47–67%). Patients with moderate to advanced disease per D_{LCO} had an elevated ^{129}Xe VDP (mean VDP, 21.7%; 95% CI, 15.3–28.0%) as compared with those with mild disease (mean VDP, 11.9%; 95% CI, 7.8–16.0%; $P = 0.02$). There was no significant difference in ^{129}Xe ADC between the patients with mild LAM (mean ADC, 0.038 cm^2/s; 95% CI, 0.027–0.048 cm^2/s) and those with moderate to advance disease (mean ADC, 0.050 cm^2/s; 95% CI, 0.043–0.057 cm^2/s; $P = 0.12$).

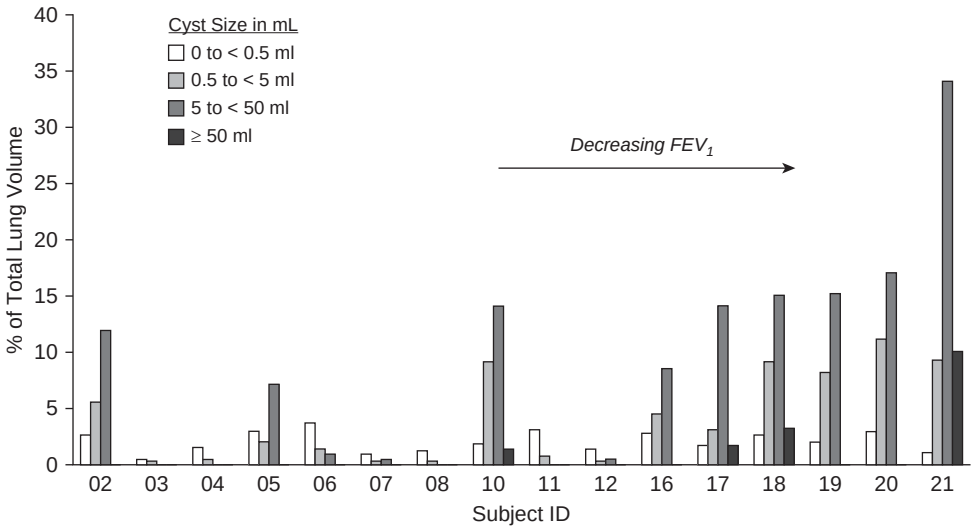

Figure 4. Cyst size analysis for the 16 patients with lymphangioleiomyomatosis with recent clinically obtained computed tomography scans. For each subject, cyst size is sorted into four bins: 0 to <0.5 ml (white bars), 0.5 to <5 ml (light gray bars), 5 to <50 ml (dark gray bars), and ⩾50 ml (black bars) and expressed as a percentage of the total lung volume. FEV_1 = forced expiratory volume in 1 second.

Cyst Ventilation with Co-registered ^{129}Xe MRI and CT

Sixteen of the patients with LAM had recent (<1 yr) clinical CT scans available for analysis; volume percentage of cystic lung from CT scan is listed in Table 1 for these patients. The mean volume of cystic lung was 645 ml (95% CI, 269–1,021 ml) for this group, which corresponded to an average of 15.9% (95% CI, 8.0–23.9%) of total lung volume. As Figure 4 demonstrates, subjects with a lower FEV_1 generally had a greater percentage of cystic lung (i.e., −900 HU threshold in CT scan) and a greater volume of larger cysts (e.g., cysts between 5–50 ml and >50 ml in size, as seen in subjects 17–21). Cystic lung volume percentage from CT scan was strongly correlated with FEV_1 ($r = -0.69$, $P = 0.003$), FEV_1/FVC ratio ($r = -0.77$, $P = 0.0007$), and D_{LCO} ($r = -0.88$, $P < 0.001$).

Figure 5 demonstrates the co-registered ^{129}Xe MRI and CT approach used to assess regional cyst ventilation in three representative subjects with cyst ventilation identified as "poor," "average," or "hyperventilated" in the ^{129}Xe images, and for several example cysts (numbered for each subject), cyst volume from CT scan and percentage ^{129}Xe ventilation is measured. Although cystic lung volume from CT imaging was correlated with ^{129}Xe VDP ($r = 0.58$, $P = 0.02$) and ADC ($r = 0.71$, $P = 0.007$), LAM cyst ventilation was complex and heterogeneous, and there was wide variability in the percentage ^{129}Xe ventilation within the cysts. For example, in subject 03 (Figure 5, top row), two small focal cysts are measured, and although they both have "average" ^{129}Xe ventilation per the analysis, the measured ventilation within the cysts is very different: 108% versus 61% of the normalized ^{129}Xe signal. In subject 16 (Figure 5, middle row), cysts 5 and 6 are relatively larger yet appear to ventilate better than other smaller cysts in the same ^{129}Xe image. In the images shown, subjects 16 and 17 (Figure 5, middle and bottom rows) each have an approximately 13-ml cyst identified by CT scan (cyst 3 in each case); the ^{129}Xe ventilation within that cyst for subject 16 is 95%, but it is only 49% for subject 17. LAM cyst ventilation was heterogeneous not only within an individual patient but also across similarly sized cysts in different subjects with LAM, and these complex regional differences in cyst ventilation can be quantified using hyperpolarized ^{129}Xe MRI.

Discussion

The most important findings from this study are that LAM cyst ventilation is heterogeneous and that in patients with mild disease (i.e., either FEV_1 or D_{LCO} equal to or exceeding 80% predicted), hyperpolarized ^{129}Xe MRI was sensitive to ventilation deficits and alveolar airspace dilation. The co-registered ^{129}Xe MRI and CT imaging analysis showed that cyst ventilation is complex and heterogeneous, even across similarly sized cysts. In total, these results support the regional sensitivity of ^{129}Xe MRI techniques to ventilation deficits and alveolar-microstructural changes in cystic lung disease due to LAM. We conclude that greater cyst volume percentage is associated with lower FEV_1 and a greater percentage of cysts with poor ventilation.

There are several limitations of the study and of the ^{129}Xe MRI technique. There was no age-matched control group presented in this study; thus, the ^{129}Xe VDP and ADC comparisons are made to previously reported values. The ^{129}Xe images have a larger voxel size relative to CT scans and are susceptible to partial-volume averaging, especially for smaller, isolated cysts, which can lead to overestimation of cyst ventilation. Indeed, many of the relatively smaller cysts in the CT images showed average ^{129}Xe ventilation when corrected for slice thickness. In the future, ^{129}Xe images with higher spatial resolution acquired with 3D spiral techniques could mitigate this. Furthermore, ADC can only be measured in regions of the lung that receive enough gas to make the measurement; thus larger, focal nonventilated cysts primarily observed in the advanced cases were excluded from the ADC measurement. However, inclusion of these regions would only further increase

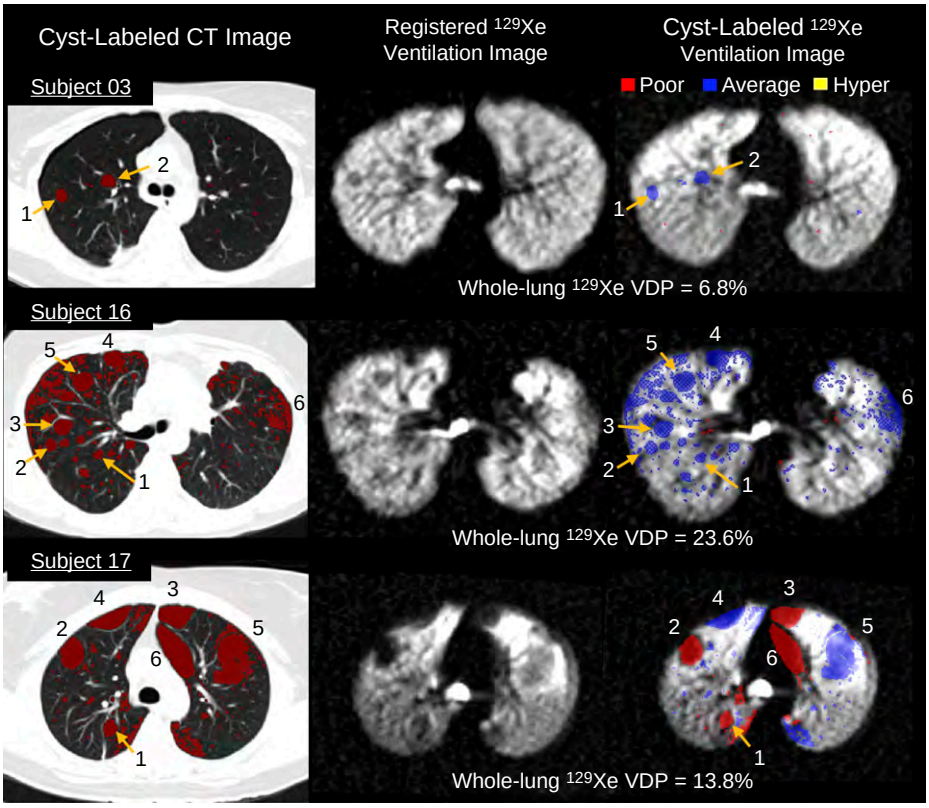

Individual Cyst Ventilation

Cyst #	Size (mL)	Normalized % ^{129}Xe Ventilation
1	0.73	108%
2	1.16	61%

Cyst #	Size (mL)	Normalized % ^{129}Xe Ventilation
1	3.4	79%
2	4.8	100%
3	13.2	95%
4	14.3	83%
5	18.8	106%
6	25.2	104%

Cyst #	Size (mL)	Normalized % ^{129}Xe Ventilation
1	3.5	50%
2	10.5	28%
3	13.9	49%
4	38.3	87%
5	42.4	110%
6	53.0	8%

Figure 5. Co-registered ^{129}Xe ventilation magnetic resonance imaging and computed tomography (CT) analysis to investigate regional lymphangioleiomyomatosis cyst ventilation. For each subject, a single cyst labeled CT image (i.e., −900 Hounsefield unit threshold), a CT-registered ^{129}Xe ventilation image, and a cyst-labeled ^{129}Xe ventilation image are shown identifying which cysts have poor ventilation (red), average ventilation (blue), or hyperventilation (yellow), with arrows pointing to individually numbered cysts for each subject. The fourth column shows cyst size and normalized percentage of ^{129}Xe ventilation for each of the numbered cysts in the CT and ^{129}Xe images. VDP = ventilation defect percentage.

the average ADC values. Region-of-interest analysis of the noncystic regions revealed that many ^{129}Xe ADC values were on par with what was expected for a given subject's age (17). Nonetheless, the global average alveolar airspace enlargement observed across the spectrum of LAM disease severity was an interesting finding and demonstrates the utility of ^{129}Xe MRI, specifically ADC, as a noninvasive method to assess alveolar airspace size *in vivo*.

These results have several important implications for the future. The finding that patients with normal spirometry have detectable ventilation and airspace-dilation abnormalities on ^{129}Xe MRI suggests that this modality might be a useful screening test to detect early disease. This is especially true for the tuberous sclerosis complex (TSC) population, which is at a particularly increased risk for the development of LAM (34). Current TSC guidelines recommend screening for LAM by a high-resolution CT scan in women ⩾18 years of age (35), and serial follow-up or screening scans every 3 to 5 years. This recommendation is associated with a significant cumulative ionizing radiation burden, and the availability of MRI techniques that can identify early cystic change and follow disease progression could serve to mitigate this risk. Early ^{129}Xe MRI assessment of disease burden in patients with LAM with and without TSC could facilitate treatment decisions regarding initiation of mammalian target of rapamycin (mTOR) inhibitor therapy in patients with normal PFTs. A recent analysis of National Heart, Lung, and Blood Institute LAM Registry data has shown that quantitative assessment of disease severity as measured by the degree of cyst profusion on CT imaging is associated with the future rate of decline of FEV_1 (36), further supporting the potential role of imaging-based assessments as prognostic biomarkers and decision-making tools. The relative ventilation of cysts may also relate to rapid decline and is the subject of an ongoing study.

^{129}Xe MRI has potential as a longitudinal disease-monitoring tool to assess the trajectory of disease progression and response to treatment. Although the correlation of ^{129}Xe MRI findings with PFTs shown here is promising, the value of longitudinal ^{129}Xe MRI monitoring needs to be assessed in prospective studies, as is currently being conducted in a substudy of the MILED (Multicenter Interventional LAM Early Disease) trial (NCT03150914, www.clinicaltrials.gov). Once validated, ^{129}Xe MRI could provide a sensitive, noninvasive, quantitative, and largely effort-independent disease monitoring tool that is free from the risks associated with ionizing radiation.

There is a critical need to develop novel remission-inducing treatment regimens in LAM and to develop sensitive biomarkers to serve as surrogate end points in clinical trials. FEV_1 change, the primary end point

in the MILES trial (37), suffers from multiple limitations, most notably the high degree of inter- and intratest variability that can result from inconsistent patient effort and technician-dependent test quality (38). Moreover, with the advent of sirolimus as an effective suppressive therapy, ^{129}Xe MRI could prove useful for demonstrating an incremental lung ventilation effect of candidate therapies in sirolimus combination trials–an endpoint that may not be feasible using FEV_1, given the large sample sizes that would be required. Development of sensitive quantitative imaging biomarkers such as ^{129}Xe MRI that can reliably detect and measure treatment effects, especially in patients with mild disease and normal PFTs, may accelerate future trials and facilitate optimal patient management in LAM.

Conclusions

In this first report of ^{129}Xe MRI in LAM, ventilation deficits and alveolar airspace dilation were noted in patients with LAM with normal spirometry, supporting ^{129}Xe MRI as a sensitive method for detecting the earliest physiological manifestations of LAM. There was considerable regional ventilation heterogeneity even across patients with similarly sized cysts. Quantitative imaging techniques such as ^{129}Xe MRI that reduce ionizing radiation exposure allow for more frequent imaging and have the potential to serve as end points for clinical trials, which would be beneficial in LAM and other rare lung disease populations where patient numbers are limited. ■

Author disclosures are available with the text of this article at www.atsjournals.org.

References

1 Johnson SR, Cordier JF, Lazor R, Cottin V, Costabel U, Harari S, *et al*.; Review Panel of the ERS LAM Task Force. European Respiratory Society guidelines for the diagnosis and management of lymphangioleiomyomatosis. *Eur Respir J* 2010;35:14–26.

2 Gupta N, Finlay GA, Kotloff RM, Strange C, Wilson KC, Young LR, *et al*.; ATS Assembly on Clinical Problems. Lymphangioleiomyomatosis diagnosis and management: high-resolution chest computed tomography, transbronchial lung biopsy, and pleural disease management. An Official American Thoracic Society/Japanese Respiratory Society Clinical Practice Guideline. *Am J Respir Crit Care Med* 2017;196:1337–1348.

3 McCormack FX, Gupta N, Finlay GR, Young LR, Taveira-DaSilva AM, Glasgow CG, *et al*.; ATS/JRS Committee on Lymphangioleiomyomatosis. Official American Thoracic Society/Japanese Respiratory Society Clinical Practice Guidelines: lymphangioleiomyomatosis diagnosis and management. *Am J Respir Crit Care Med* 2016;194: 748–761.

4 Gevenois PA, De Vuyst P, de Maertelaer V, Zanen J, Jacobovitz D, Cosio MG, *et al*. Comparison of computed density and microscopic morphometry in pulmonary emphysema. *Am J Respir Crit Care Med* 1996;154:187–192.

5 Theilig D, Doellinger F, Kuhnigk JM, Temmesfeld-Wollbrueck B, Huebner RH, Schreiter N, *et al*. Pulmonary lymphangioleiomyomatosis: analysis of disease manifestation by region-based quantification of lung parenchyma. *Eur J Radiol* 2015;84:732–737.

6 Crausman RS, Lynch DA, Mortenson RL, King TE Jr, Irvin CG, Hale VA, *et al*. Quantitative CT predicts the severity of physiologic dysfunction in patients with lymphangioleiomyomatosis. *Chest* 1996;109: 131–137.

7 Washko GR, Parraga G. Imaging Biomarkers in lymphangioleiomyomatosis clinical trials: a wolf in sheep's clothing? *Ann Am Thorac Soc* 2016;13: 307–308.

8 Argula RG, Kokosi M, Lo P, Kim HJ, Ravenel JG, Meyer C, *et al*.; MILES Study Investigators. A novel quantitative computed tomographic analysis suggests how sirolimus stabilizes progressive air trapping in lymphangioleiomyomatosis. *Ann Am Thorac Soc* 2016;13: 342–349.

9 Schmithorst VJ, Altes TA, Young LR, Franz DN, Bissler JJ, McCormack FX, *et al*. Automated algorithm for quantifying the extent of cystic change on volumetric chest CT: initial results in Lymphangioleiomyomatosis. *AJR Am J Roentgenol* 2009;192: 1037–1044.

10 Avila NA, Chen CC, Chu SC, Wu M, Jones EC, Neumann RD, *et al*. Pulmonary lymphangioleiomyomatosis: correlation of ventilation-perfusion scintigraphy, chest radiography, and CT with pulmonary function tests. *Radiology* 2000;214:441–446.

11 Higano N, Hahn A, Tkach JA, Cao X, Walkup LL, Thomen RP, *et al*. Retrospective respiratory self-gating and removal of bulk motion in pulmonary UTE MRI of neonates and adults. *Magn Reson Med* 2017; 77:1284–1295.

12 Hahn AD, Higano NS, Walkup LL, Thomen RP, Cao X, Merhar SL, *et al*. Pulmonary MRI of neonates in the intensive care unit using 3D ultrashort echo time and a small footprint MRI system. *J Magn Reson Imaging* 2017;45:463–471.

13 Roach DJ, Crémillieux Y, Fleck RJ, Brody AS, Serai SD, Szczesniak RD, *et al*. Ultrashort echo-time magnetic resonance imaging is a sensitive method for the evaluation of early cystic fibrosis lung disease. *Ann Am Thorac Soc* 2016;13:1923–1931.

14 Roach DJ, Crémillieux Y, Serai SD, Thomen RP, Wang H, Zou Y, *et al*. Morphological and quantitative evaluation of emphysema in chronic obstructive pulmonary disease patients: a comparative study of MRI with CT. *J Magn Reson Imaging* 2016;44:1656–1663.

15 Ma W, Sheikh K, Svenningsen S, Pike D, Guo F, Etemad-Rezai R, *et al*. Ultra-short echo-time pulmonary MRI: evaluation and reproducibility in COPD subjects with and without bronchiectasis. *J Magn Reson Imaging* 2015;41:1465–1474.

16 Sheikh K, Guo F, Capaldi DP, Ouriadov A, Eddy RL, Svenningsen S, *et al*.; Canadian Respiratory Research Network. Ultrashort echo time MRI biomarkers of asthma. *J Magn Reson Imaging* 2017;45: 1204–1215.

17 Kaushik SS, Cleveland ZI, Cofer GP, Metz G, Beaver D, Nouls J, *et al*. Diffusion-weighted hyperpolarized 129Xe MRI in healthy volunteers and subjects with chronic obstructive pulmonary disease. *Magn Reson Med* 2011;65:1154–1165.

18 Walkup LL, Woods JC. Translational applications of hyperpolarized 3He and 129Xe. *NMR Biomed* 2014;27:1429–1438.

19 Ebner L, Kammerman J, Driehuys B, Schiebler ML, Cadman RV, Fain SB. The role of hyperpolarized ^{129}xenon in MR imaging of pulmonary function. *Eur J Radiol* 2017;86:343–352.

20 Thomen RP, Walkup LL, Roach DJ, Cleveland ZI, Clancy JP, Woods JC. Hyperpolarized ^{129}Xe for investigation of mild cystic fibrosis lung disease in pediatric patients. *J Cyst Fibros* 2017;16:275–282.

21 Kanhere N, Couch MJ, Kowalik K, Zanette B, Rayment JH, Manson D, *et al*. Correlation of lung clearance index with hyperpolarized ^{129}Xe magnetic resonance imaging in pediatric subjects with cystic fibrosis. *Am J Respir Crit Care Med* 2017;196:1073–1075.

22 Walkup LL, Thomen RP, Akinyi TG, Watters E, Ruppert K, Clancy JP, *et al*. Feasibility, tolerability and safety of pediatric hyperpolarized ^{129}Xe magnetic resonance imaging in healthy volunteers and children with cystic fibrosis. *Pediatr Radiol* 2016;46:1651–1662.

23 Shukla Y, Wheatley A, Kirby M, Svenningsen S, Farag A, Santyr GE, *et al*. Hyperpolarized 129Xe magnetic resonance imaging: tolerability in healthy volunteers and subjects with pulmonary disease. *Acad Radiol* 2012;19:941–951.

24 Svenningsen S, Kirby M, Starr D, Leary D, Wheatley A, Maksym GN, *et al*. Hyperpolarized (3) He and (129) Xe MRI: differences in asthma before bronchodilation. *J Magn Reson Imaging* 2013;38: 1521–1530.

25 Dregely I, Mugler JP III, Ruset IC, Altes TA, Mata JF, Miller GW, *et al*. Hyperpolarized Xenon-129 gas-exchange imaging of lung microstructure: first case studies in subjects with obstructive lung disease. *J Magn Reson Imaging* 2011;33:1052–1062.

26 Driehuys B, Martinez-Jimenez S, Cleveland ZI, Metz GM, Beaver DM, Nouls JC, *et al*. Chronic obstructive pulmonary disease: safety and tolerability of hyperpolarized 129Xe MR imaging in healthy volunteers and patients. *Radiology* 2012;262:279–289.
27 Walkup LL, Thomen R, Freeman M, Cleveland Z, McCormack FX, Woods JC. Hyperpolarized 129Xe Ventilation and Diffusion MRI of Lymphangioleiomyomatosis [abstract]. *Am J Respir Crit Care Med* 2017;195:A6469.
28 Roach D, Walkup L, Hall C, Thomen RP, McCormack FX, Gupta N, *et al*. Quantification of cyst ventilation using hyperpolarized 129Xe MRI Correlates with pulmonary function tests in patients with lymphangioleiomyomatosis [abstract]. *Am J Respir Crit Care Med* 2018;196:A5924.
29 Loew W, Thomen R, Pratt R, Cleveland ZI, Dumoulin C, Woods JC, *et al*. A volume saddle coil for hyperpolarized 129Xe lung imaging. *Proc Intl Soc Magn Reson Med* 2015;23:1507.
30 Yushkevich PA, Piven J, Hazlett HC, Smith RG, Ho S, Gee JC, *et al*. User-guided 3D active contour segmentation of anatomical structures: significantly improved efficiency and reliability. *Neuroimage* 2006;31:1116–1128.
31 Avants BB, Tustison NJ, Song G, Cook PA, Klein A, Gee JC. A reproducible evaluation of ANTs similarity metric performance in brain image registration. *Neuroimage* 2011;54:2033–2044.
32 Virgincar RS, Cleveland ZI, Kaushik SS, Freeman MS, Nouls J, Cofer GP, *et al*. Quantitative analysis of hyperpolarized 129Xe ventilation imaging in healthy volunteers and subjects with chronic obstructive pulmonary disease. *NMR Biomed* 2013;26:424–435.
33 Ouriadov A, Farag A, Kirby M, McCormack DG, Parraga G, Santyr GE. Lung morphometry using hyperpolarized (129) Xe apparent diffusion coefficient anisotropy in chronic obstructive pulmonary disease. *Magn Reson Med* 2013;70:1699–1706.
34 Cudzilo CJ, Szczesniak RD, Brody AS, Rattan MS, Krueger DA, Bissler JJ, *et al*. Lymphangioleiomyomatosis screening in women with tuberous sclerosis. *Chest* 2013;144:578–585.
35 Krueger DA, Northrup H; International Tuberous Sclerosis Complex Consensus Group. Tuberous sclerosis complex surveillance and management: recommendations of the 2012 International Tuberous Sclerosis Complex Consensus Conference. *Pediatr Neurol* 2013;49: 255–265.
36 Gupta N, Lee H-S, Ryu JH, Taveira-DaSilva AM, Beck GJ, Lee J-C, *et al*.; NHLBI LAM Registry Group. The NHLBI LAM Registry: prognostic physiologic and radiologic biomarkers emerge from a 15-year prospective longitudinal analysis. *Chest* 2019;155:288–296.
37 McCormack FX, Inoue Y, Moss J, Singer LG, Strange C, Nakata K, *et al*.; National Institutes of Health Rare Lung Diseases Consortium; MILES Trial Group. Efficacy and safety of sirolimus in lymphangioleiomyomatosis. *N Engl J Med* 2011;364:1595–1606.
38 Pellegrino R, Viegi G, Brusasco V, Crapo RO, Burgos F, Casaburi R, *et al*. Interpretative strategies for lung function tests. *Eur Respir J* 2005;26: 948–968.